The Astrophysical Journal, 644:1028–1039, 2006 June 20

NUCLEOSYNTHESIS IN EARLY SUPERNOVA WINDS. II. THE ROLE OF NEUTRINOS

J. Pruet and R. D. Hoffman
N Division, Lawrence Livermore National Laboratory, P.O. Box 808, Livermore, CA 94550;
pruet1@llnl.gov, rdhoffman@llnl.gov

S. E. Woosley
Department of Astronomy and Astrophysics, University of California, Santa Cruz, CA 95064; woosley@ucolick.org

and

H.-T. Janka and R. Buras
Max-Planck-Institut für Astrophysik, Karl-Schwarzschild-Strasse 1, 85741 Garching, Germany;
thj@mpa-garching.mpg.de, rburas@mpa-garching.mpg.de
Received 2005 November 7; accepted 2006 March 1

ABSTRACT

One of the outstanding unsolved riddles of nuclear astrophysics is the origin of the so-called *p*-process nuclei from $A = 92$ to 126. Both the lighter and heavier *p*-process nuclei are adequately produced in the neon and oxygen shells of ordinary Type II supernovae, but the origin of these intermediate isotopes, especially ^{92,94}Mo and ^{96,98}Ru, has long been mysterious. Here we explore the production of these nuclei in the neutrino-driven wind from a young neutron star. We consider such early times that the wind still contains a proton excess because the rates for ν_e and positron captures on neutrons are faster than those for the inverse captures on protons. Following a suggestion by Fröhlich and coworkers, we also include the possibility that—in addition to the protons, α-particles, and heavy seed—a small flux of neutrons is maintained by the reaction $p(\bar{\nu}_e, e^+)n$. This flux of neutrons is critical in bridging the long waiting points along the path of the *rp*-process by (n, p) reactions. Using the unmodified ejecta histories from a recent two-dimensional supernova model by Janka and coworkers, we find synthesis of *p*-rich nuclei up to ^{102}Pd, although our calculations do not show efficient production of ^{92}Mo. If the entropy of these ejecta is increased by a factor of 2, the synthesis extends to ^{120}Te. Still larger increases in entropy, which might reflect the role of magnetic fields or vibrational energy input neglected in the hydrodynamical model, result in the production of nuclei up to $A \approx 170$. Elements synthesized in these more extreme outflows include numerous *s*- and *p*-process nuclei, and even some *r*-process nuclei can be synthesized in these proton-rich conditions.

Subject headings: nuclear reactions, nucleosynthesis, abundances — supernovae: general

1. INTRODUCTION

Burbidge et al. (1957) attributed the production of the isotopes heavier than the iron group to three processes of nucleosynthesis: the *r*- and *s*-processes of neutron addition, and the *p*-process of proton addition. The conditions they specified for the *p*-process, proton densities $\rho X_p \sim 10^2$ g cm^{-3} and temperatures $T \sim (2\text{–}3) \times 10^9$ K, were difficult to realize in nature and so other processes and sites were sought. Arnould (1976) and Woosley & Howard (1978) attributed the production of the *p*-process nuclei to photodisintegration, a series of (γ, n), (γ, p), and (γ, α) reactions flowing downward through radioactive proton-rich progenitors from lead to iron. Their "γ-process" operated on previously existing *s*-process seed in the star to make the *p*-process and was thus "secondary" in nature (or even "tertiary," since the *s*-process itself is secondary). It could only happen in a star made from the ashes of previous stars that had made the *s*-process.

Arnould (1976) suggested hydrostatic oxygen burning in massive stars as the site where the necessary conditions were realized; Woosley & Howard (1978), who discovered the relevant nuclear flows independently, discussed explosive oxygen and neon burning in a Type II supernova (SN) as the likely site. Over the years, increasingly refined calculations showed that a portion of the *p*-nuclei could actually be produced as Woosley & Howard described (e.g., Rauscher et al. 2002). A nagging deficiency of *p*-process production in the mass range $A = 92\text{–}126$ still persisted, however. The production of ^{92,94}Mo posed a particular problem, since, unless the star had previously experienced a strong *s*-process, enhancing the abundance of seed above $A = 95$, there simply was not enough seed. In massive stars the weak component of the *s*-process does not go above mass 90, so the necessary seed enhancement does not occur.

Hoffman et al. (1996) found that large abundances of some *p*-nuclei, and ^{92}Mo in particular, could be synthesized in the neutrino-powered wind blowing from a young neutron star (see also Duncan et al. 1986). While this wind had chiefly been seen as a way of making the *r*-process (Woosley et al. 1994), for electron mole numbers $Y_e \approx 0.485$, the *p*-nuclei ^{64}Zn, ^{74}Se, ^{78}Kr, ^{84}Sr, and ^{92}Mo were produced in great abundance. It is important to note in this regard that, while $Y_e = 0.485$ is nominally neutron-rich ($Y_e = 0.5$ corresponds to neutron, proton equality), it is still a lot more proton-rich than the *p*-nuclei themselves (Z/A for ^{92}Mo $= 0.457$), so the nucleonic gas contained some free protons. The *p*-nuclei here were also primary, in the sense that a star with no initial metallicity would still make the same composition in its neutrino wind. There were potential problems, however, in that the ejection of only a small amount of mass with Y_e just a little lower than 0.485 resulted in disastrous overproduction of $N = 50$ nuclei such as ^{88}Sr, ^{89}Y, and ^{90}Zr. Also, the neutron-rich wind failed to produce adequate amounts of *p*-process nuclei above $A = 92$. Although this paper focuses on early proton-rich outflows, the SN model we study is calculated to eject a sizable amount of neutron-rich material. It remains to be seen if very recent simulations predict neutron-rich outflows

that satisfy the conditions needed for efficient synthesis of ^{92}Mo, or if neutrino interactions facilitate production of ^{92}Mo in the neutron-rich ejecta predicted by these models (Fuller & Meyer 1995).

Based on calculations by Jim Wilson, Qian & Woosley (1996) pointed out that Y_e in the wind would naturally evolve through the points necessary to make these p-nuclei and would actually start with a value greater than 0.5. As other detailed models for core-collapse SNe became available, nucleosynthesis was explored in this "hot, proton-rich bubble" by Pruet et al. (2005) and Fröhlich et al. (2004, 2006). The latter two studies found substantial production of nuclei up to $A = 84$, including some nuclei traditionally attributed to the p-process. It seems probable that these winds have also contributed appreciably to the solar abundances of ^{45}Sc, ^{49}Ti, and ^{64}Zn, and, possibly in a measurable way, to other rare abundances in metal-poor stars. However, since these same nuclei were already made by other processes (Woosley et al. 2002; Rauscher et al. 2002), there seemed to be no clear diagnostic of the proton-rich wind.

Jordan & Meyer (2004) were the first to show that explosive nucleosynthesis in rapidly expanding proton-rich outflows can give rise to heavy p-process and even r-process nuclei. In the conditions studied by those authors, this arises because when the entropy is sufficiently high and the fluid expansion timescale is sufficiently short, reactions that form α-particles fall out of nuclear statistical equilibrium. As a result, a relatively large abundance of free nucleons survives until low temperatures, at which point they can be efficiently captured on heavy seed nuclei. This is similar in some ways to the nucleosynthesis studied here, except that in the process proposed by Fröhlich et al., neutrinos (rather than a freezeout of light ion reactions) are responsible for providing free nucleons at low temperatures.

Here, following the suggestion of Fröhlich et al. (2006), we have revisited our calculations of the proton-rich wind, including—in addition to the proton captures—the effect of a neutron flux created by $p(\bar{\nu}_e,\ e^+)n$. These neutrons have the effect of bridging the long-lived isotopes along the path of the rp-process by (n, p) reactions and accelerating the flow to heavier elements. For our standard assumptions regarding expansion rate and neutrino fluxes (Pruet et al. 2005), we find substantial production of p-process nuclei up to Pd, whereas previously the heaviest major production was Zn. If the entropy of the expansion is artificially increased by a factor of 3 to account for extra energy deposition in the wind (Qian & Woosley 1996), magnetic confinement (Thompson 2003), or Alfvén wave dissipation (Suzuki & Nagataki 2005), the production of p-nuclei extends up to $A = 170$.

It is interesting to note that the relevant conditions, $\rho X_p \approx 10^3$ g cm^{-3} and $T = 2 \times 10^9$ K, resemble those originally proposed for the p-process by B^2FH. Key differences, however, are that all the species produced here are primary, and the process occurs on a shorter timescale—just a few seconds—owing to the "effective" acceleration of weak decays by (n, p) reactions.

2. NUCLEOSYNTHESIS IN AN EXPLODING 15 $M_\odot$ STAR

Our fiducial model for exploring nucleosynthesis in the proton-rich wind is the explosion of a 15 $M_\odot$ star (Janka et al. 2003; Buras et al. 2006). An earlier paper (Pruet et al. 2005, hereafter Paper I) studied nucleosynthesis in this same model but did not account for the influence of neutrino interactions. The present study includes charged-current capture on free nucleons (McLaughlin & Fuller 1995) and neutral-current spallation of nucleons from α-particles (Woosley et al. 1990; Meyer 1995). Many other details of the SN model and associated nuclear-network calculations relevant to this work can be found in Paper I.

The ejecta of the deepest layers of the SN can be divided into two categories: hot bubble ejecta and winds. Material in the hot bubble originates from a region outside the neutron star that is driven convectively unstable by neutrino heating. This material does not have to escape the deep gravitational well found at the neutron star surface. As a result, modest conditions characterize these outflows: $s/k_b \sim 20-30$ and $Y_e \lesssim 0.52$. Winds originate from the surface of the neutron star and are pushed outward along gentle pressure gradients caused by neutrino heating (Duncan et al. 1986; Qian & Woosley 1996). These outflows have relatively high entropies ($s/k_b \sim 50-80$), high electron fractions (Y_e as large as 0.57), and short initial expansion timescales. Tables 2 and 3 in Paper I provide a brief summary of initial conditions in different bubble and wind trajectories.

In the absence of neutrinos, very little synthesis occurs in the early proton-rich outflows for nuclei heavier than $A = 64$. Compared to observed solar abundances, proton-rich winds that are not subject to a neutrino fluence are copious producers of ^{45}Sc and ^{46,49}Ti (Paper I). Bubble trajectories, on the other hand, tend to favor the synthesis of ^{64}Zn, ^{46,49}Ti, and some Co or Ni isotopes. The nuclear flow stops at ^{64}Ge for two reasons: the long weak decay lifetime (with respect to the expansion timescale of the neutrino winds) of this and other even-Z even-N "waiting point" nuclei, and the small Q values for proton capture on these nuclei.

2.1. *Estimating the Late-time Evolution*

The simulations of Janka et al. (2003) followed the explosion of the SN in two dimensions until about 450 ms after core bounce. At this time, typical temperatures in the bubble trajectories were around 4 billion degrees. At the end of the two-dimensional simulation, the SN was mapped onto a one-dimensional grid. The subsequent evolution of the SN, including winds emitted by the neutron star, was followed until about 1300 ms after core bounce. At this last time, typical asymptotic temperatures in the early wind were just over 2 billion degrees.

Since most of the interesting nucleosynthesis occurs for $T_9 \leq 2$, it is necessary to extrapolate outflow conditions to later times. Details of the extrapolation were described in § 2.2 of Paper I, which considered two estimates. In the first, the expansion already calculated is assumed to continue homologously with no deceleration. This gives a useful lower bound on the expansion timescale. However, in reality the outflow will quickly catch up to the outgoing shock. It is more reasonable then to assume that escaping matter enters a phase in which it moves with the shock speed. Conditions for this can be estimated from one-dimensional SN simulations.

For the present paper we focus on the more realistic extrapolation that mimics the late-time slowing of the wind. The temperature and density evolution was extrapolated as in Paper I. Specifically, the trajectories found by Janka et al. (2003) were smoothly merged with those calculated for the inner zone of the same 15 $M_\odot$ star by Woosley & Weaver (1995). To avoid discontinuities in the entropy at the time when the two calculations were matched, the density in the previous one-dimensional calculation was changed to match that in the trajectories found by Janka et al. Our procedure likely leads to an underestimate of the expansion timescale at late times because the explosion energy and shock velocity in the calculations of Woosley & Weaver were somewhat larger than in the more recent two-dimensional simulations.

To obtain the integrated neutrino exposure seen by outflowing material, it is also necessary to make assumptions about the evolution of the radial velocity. In all cases, it was assumed that the

TABLE 1
PARAMETERS CHARACTERIZING THE DIFFERENT NEUTRINO SPECIES AT 925 ms POST–CORE BOUNCE IN THE SIMULATION OF JANKA ET AL. (2003)

Species	T_ν (MeV)	L_ν (10^{51} ergs s^{-1})
ν_e	3.86	17.9
$\bar{\nu}_e$	4.62	17.7
ν_x[a]	4.9	24.5

[a] Represents any of the μ and τ neutrinos and antineutrinos.

radial velocity at times greater than those followed in the simulations was constant at $v_r = 4 \times 10^8$ cm s^{-1}. This is close to the velocity of the outgoing shock in the two-dimensional calculation of this fairly low energy explosion. Again, there may be some inconsistency between our treatment of the late-time expansion and our adopted asymptotic radial velocity. A more sophisticated approach might scale the expansion time estimated from the calculations of Woosley & Weaver to reflect the relatively small shock velocity found in the two-dimensional simulations. It is shown in § 2.3 that our calculations for nucleosynthesis are relatively insensitive to changes in the late-time outflow velocity.

In order to include the influence of the neutrinos from the cooling neutron star, information about the spectral and temporal evolution of these neutrinos is needed. For the neutrino temperatures and luminosities, we used the same values calculated at approximately 1 s in the simulations of Janka et al. (2003). These values are shown in Table 1 and are assumed to remain constant. This may be a questionable assumption; neutrino spectra actually harden, and their luminosities fall as the neutron star shrinks. However, it is estimated that uncertainties in the extrapolation of trajectories to low temperatures are greater than, or at least cannot be simply disentangled from, uncertainties arising from our simple treatment of the neutrino spectral evolution. To see why, consider the evolution of a typical wind trajectory. For definiteness we concentrate on the trajectory labeled 6 in Table 2, which is also the trajectory for which neutrino interactions play the most interesting role. It takes about 180 ms for material in trajectory 6 to cool from 10 to 2.24 billion degrees, the lowest temperature followed by the simulations of Janka et al. During this time the luminosity falls by approximately 5%. At the beginning of the extrapolated portion of the trajectory (when $T =$ 2.24 billion degrees) the radius of the outflowing material is 2.2×10^8 cm. With an assumed radial velocity of 4×10^8 cm s^{-1}, the radius at a time 1 s later, when the temperature has fallen to 1.5 billion degrees and rapid nucleosynthesis is still occurring, is 6.2×10^8 cm. This implies that radial outflow alone results in a decrease of about a factor of 8 in the local neutrino capture rate. By contrast, for a nominal neutrino evolution timescale of 3 s, the neutrino flux only falls by about 40% during this same time. In § 2.3 we study the influence of increasing the asymptotic radial velocity to 10^9 cm s^{-1}. This results in about a factor of 4 change in the local neutrino capture rates when the wind has cooled to 1.5 billion degrees — a change considerably larger than seems plausible for the change in luminosity of the neutron star during the same period.

2.2. *Results*

Figure 1 shows results of our calculations that include neutrino captures for production factors characterizing nucleosynthesis in proton-rich outflows leaving the early SN. The net production factor for an isotope i is defined here as

$$P(i) = \sum_j \frac{M_j}{M^{\rm ej}} \frac{X_j(i)}{X_{\odot,i}}. \quad (1)$$

In this equation, the sum is over all trajectories, $X_j(i)$ is the mass fraction of nuclide i in the jth trajectory, $X_{\odot,i}$ is the mass fraction of nuclide i in the Sun (Lodders 2003), M_j is the mass of the jth trajectory, and $M^{\rm ej} = 13.5\ M_\odot$ is the total mass ejected in the SN explosion.

The lower panel in Figure 1 shows production factors characterizing nucleosynthesis in just the hot bubble. This is comprised of the 40 trajectories described in Table 1 of Paper I. By comparing with Table 5 from Paper I we see that nucleosynthesis in the bubble material is not greatly changed when neutrino captures are included. This is because the bubble material is far from the neutron star and experiences few neutrino captures relative to the number of seed nuclei in this low-entropy environment. The story is much different for the early wind shown in the middle panel of Figure 1. This wind is comprised of the six trajectories defined in Table 2 of Paper I. In these outflows, neutrinos convert free protons into neutrons. Absorption of these neutrons via (n, p) reactions on long-lived nuclei along the path of the *rp*-process accelerate the nuclear flows to species as heavy as Pd. Final conditions for these wind trajectories are provided in Table 2. We defer a discussion of the nuclear flows and the potential for production of heavier elements to § 3.

For comparison, we also show, in Figure 2, the integrated results (summed over the same six wind trajectories) of calculations that do *not* include neutrino capture on protons. Apart from the neglect of neutrinos, the trajectories studied here are identical to those described in the middle panel of Figure 1. The differences are dramatic. When neutrino captures are ignored, nucleosynthesis stops some 40 mass units lower than when they are included.

TABLE 2
FINAL CONDITIONS FOR EARLY WIND OUTFLOWS

Trajectory	Y_e	s/k_b	$X(p)$	$X(\alpha)$	X_H	$X(^{56}\mathrm{Ni})$	Percent[a]	Δ_n[b]
1	0.539	54.8	0.078	0.614	0.307	0.244	80	0.2
2	0.548	58.0	0.095	0.714	0.190	0.135	71	0.4
3	0.551	76.7	0.101	0.822	0.075	0.043	57	1.7
4	0.551	71.0	0.102	0.796	0.101	0.063	62	1.1
5	0.556	74.9	0.113	0.831	0.054	0.025	46	2.9
6	0.558	76.9	0.115	0.840	0.043	0.014	33	3.2

NOTE.— At the end of the simulations $T_9 \approx 0.65$.
[a] The percentage of heavy nuclei that was ^{56}Ni.
[b] Estimate from eq. (2) of the number of neutrons created by neutrino capture at temperatures less than 3 billion degrees.

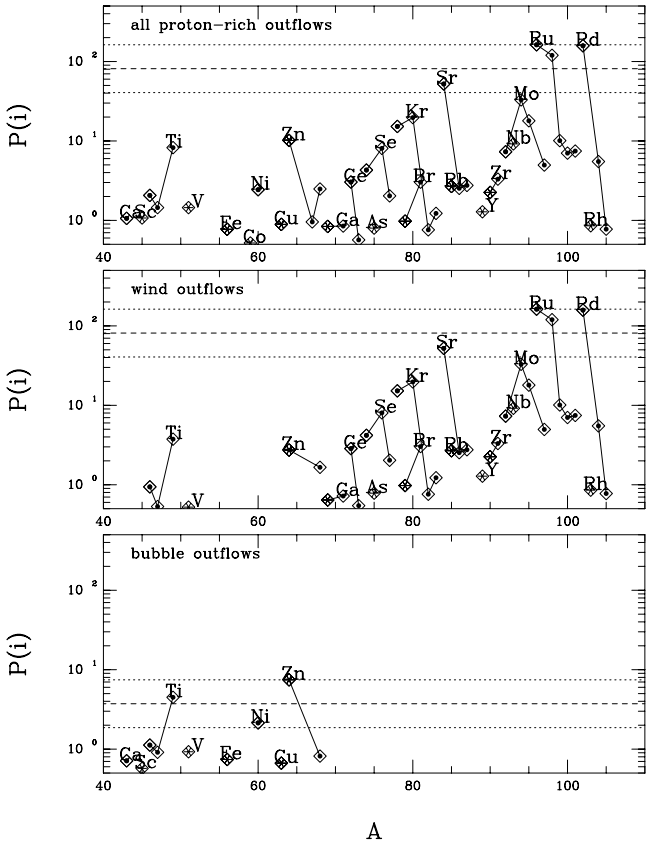

FIG. 1.—Production factors characterizing nucleosynthesis in proton-rich trajectories occurring during the explosion of the 15 $M_\odot$ star studied by Janka et al. (2003). The bottom panel gives the contribution of just the proton-rich hot bubble trajectories to the net production factors. These trajectories are characterized by the weak production of a few neutrons per heavy nucleus. The number of neutrons created by weak interactions per heavy nucleus (Δ_n) in these flows spans a range from about 0 to 0.05. The middle panel gives the contribution of just the proton-rich wind trajectories to the total nucleosynthesis. These winds are characterized by relatively high entropies and electron fractions and reach low temperatures near the neutron star. Neutrinos result in the production of between about 0.2 and 3.2 free neutrons per heavy nucleus in the wind trajectories. The top panel shows net production in all proton-rich outflows. This is the sum of the lower two panels. In each panel, solid lines connect isotopes of a given element. The most abundant isotope for a given element is indicated with an asterisk. Any isotope surrounded by a diamond indicates that it was made chiefly as a radioactive progenitor. We draw horizontal lines at the production factor value of the largest nucleus produced, and a factor of 2 and 4 less than that, respectively.

2.3. *Influence of Modest Changes to the Early Wind and Neutron Star*

Two distinct sources of uncertainty can influence calculations of nucleosynthesis presented in § 2.2. One of these relates to possible errors associated with extrapolating Janka et al.'s (2003) trajectories to late times and low temperatures. The other relates to uncertainties associated with present-day SN simulations: unaccounted-for three-dimensional effects, incomplete understanding of neutrino opacities, and so on. Here we consider the influence of modest alterations to the wind properties that might result from these two kinds of uncertainties. More extreme changes that might reflect the influence of novel physical processes operating in the early wind are explored in § 3.

Influence of a Larger Asymptotic Wind Velocity.—The SN studied by Janka et al. has a relatively low kinetic energy at infinity, 0.6×10^{51} ergs. More energetic explosions would give rise to shock velocities larger than the 4×10^8 cm s^{-1} adopted here. To estimate nucleosynthesis in more energetic SNe, we show in

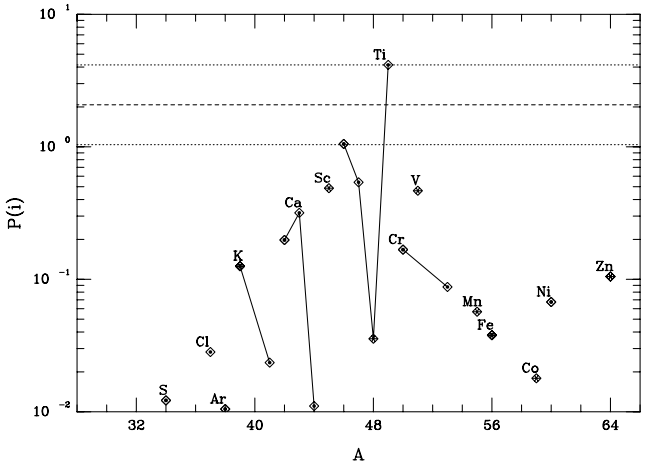

FIG. 2.—Influence of neglecting neutrino captures on nucleosynthesis in the early wind. This figure shows integrated production factors for the six wind trajectories given by the fiducial SN simulation. Apart from the neglect of neutrinos, the trajectories studied here are the same ones represented by the middle panel of Fig. 1.

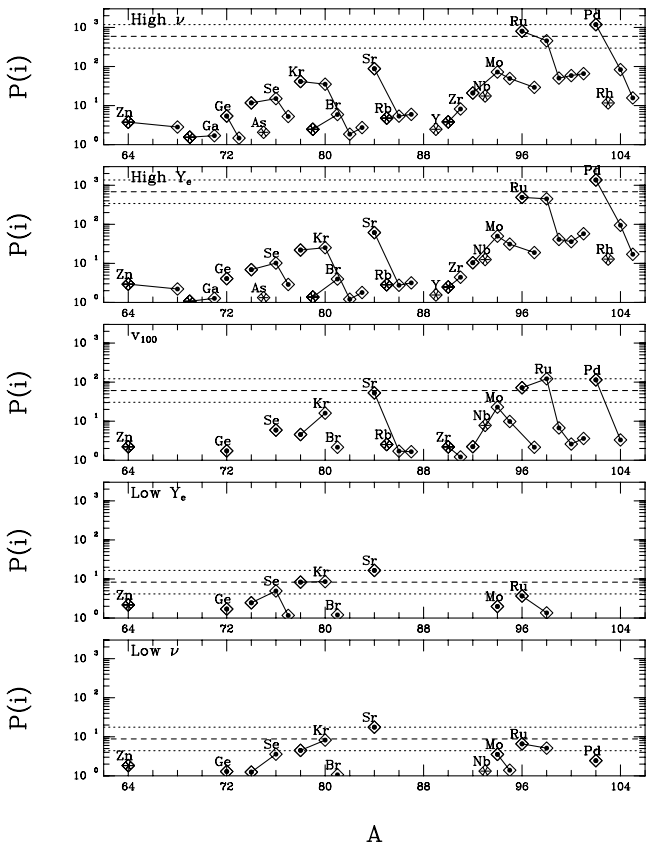

FIG. 3.—Influence of modest changes to the early wind and neutron star on nucleosynthesis. The top panel corresponds to a wind for which the charged current neutrino capture rates are twice those found by simulation. The second panel corresponds to a wind with Y_e increased by 5% relative to the value found by simulation for each of the six trajectories. The middle panel corresponds to a wind for which the asymptotic velocity is set to 10^9 cm s^{-1}. The fourth panel corresponds to a wind with Y_e decreased by 5% relative to the value found by simulation for each of the six trajectories. Finally, the bottom panel corresponds to a wind for which the charged current neutrino capture rates are half those found by simulation. Apart from the specified changes, all other characteristics of the wind for the set of calculations reflected by each panel were kept unchanged.

the middle panel of Figure 3 production factors for nuclei synthesized in a wind characterized by an asymptotic velocity of 10^9 cm s^{-1}. This is more typical of SNe with late-time kinetic energies near 10^{51} ergs. Apart from the increase in asymptotic velocity, all other properties of the six trajectories comprising the early wind were kept unchanged from those found by simulation.

By comparing with the middle panel of Figure 1, one sees that changing the asymptotic outflow velocity has a modest impact on nucleosynthesis. Yields for ^{102}Pd and ^{98}Ru are within a factor of 2 of each other for the two different outflow velocities. Production of ^{96}Ru is suppressed by a factor of a few in the high outflow velocity calculation. The modest sensitivity to asymptotic outflow velocity likely arises because most of the neutrino captures occur during the portion of the trajectory that is not extrapolated.

Effect of 5% *changes to* Y_e.—Uncertainty in the neutrino spectral evolution or the dynamics of the wind near the neutron star could affect Y_e in the wind. The second and fourth panels of Figure 3 show the influence of changing the initial electron fraction up or down by 5%. This change was applied to all six trajectories comprising the early wind. Other characteristics of these trajectories were left unchanged.

It is evident that relatively small changes to the electron fraction can have a big impact on nucleosynthesis. If Y_e is decreased by 5%, production of p-isotopes near mass 100 is lost and replaced by modest synthesis of some proton-rich Kr and Sr isotopes. A 5% increase in Y_e leads to large production of Ru and Pd isotopes. The reason for the large impact of changing Y_e can be understood in terms of the number of protons available for capturing neutrinos. The most proton-rich trajectory found by simulations had $Y_e = 0.570$. This corresponds to a mass fraction of free protons $X_p \approx 2Y_e - 1 = 0.140$. Increasing Y_e by 5% corresponds to a 40% increase in X_p.

Although uncertainties in early SN dynamics may give rise to appreciable changes in Y_e, the uncertainty in Y_e associated with extrapolating Janka et al.'s results to late times is not very large. For example, the trajectory with the largest fractional change in electron fraction was trajectory 6. This started off with $Y_e = 0.57$ and ended with $Y_e = 0.558$ (Table 2), an approximately 2% decrease. Of this 2% decrease, only a small fraction occurred during our extrapolated portion of the trajectory. This is shown in Figure 6, which illustrates the time dependence of the total number of neutrino captures on free nucleons for trajectory 6.

Changes to the Neutrino Capture Rates.—The first and last panels of Figure 3 show the influence of halving and doubling the luminosity of electron neutrinos and antineutrinos. Such large changes to the luminosities are probably unlikely, but might reflect plausible uncertainties in the local neutrino capture rate experienced by the wind. For example, the wind material might first catch up with the outgoing shock at a larger radius than found by simulations. Our neglect of the temporal evolution and finer spectral details of the neutrinos might also result in modest changes to the capture rates. From Figure 3 it can be seen that halving or doubling the charged current neutrino capture rates is roughly equivalent to decreasing or increasing Y_e by 5%.

2.4. *Implications*

Galactic chemical evolution studies indicate that production factors in the whole star for isotopes exclusively produced in core-collapse SNe must be of order 10 (Mathews et al. 1992). As noted before (Paper I; Fröhlich et al. 2006), this implies that the current simulations predict a hot bubble ejecta that could explain the origin of ^{46,49}Ti and ^{64}Zn. Implications for the early wind are more interesting. The simulations of Janka et al. (2003), together with the present estimates for the late-time character of the outflows, predict a wind that efficiently synthesizes several interesting p-nuclei. From the middle panel of Figure 1 it can be seen that the elusive isotopes ^{96,98}Ru and ^{102}Pd all have production factors that are within a factor of 2 of each other. That is, their relative proportions approximately follow those in the Sun. Overall, however, the calculations predict about 5–10 times too much yield of the most proton-rich stable Pd and Ru isotopes. In § 2.3 it was shown that small changes to the electron fraction can alleviate this overproduction.

3. NUCLEOSYNTHESIS IN MORE EXTREME CONDITIONS

In this section we consider nucleosynthesis in outflows for which neutrino, proton, and neutron-induced reactions on heavy seed can produce still heavier nuclei. This may occur because the proton to seed ratio is higher—as happens if the entropy is higher—or the production of neutrons by $p(\bar{\nu}, e^+)n$ is greater. Reasons why the entropy might be higher are discussed in the conclusions.

3.1. *Basic Considerations*

Qualitatively, the nucleosynthesis we are describing occurs in three, or possibly four, stages. First, in the outgoing wind, all neutrons combine with protons, leaving an excess of unbound protons—much like in the big bang. As this combination of α-particles and protons cools below 5×10^9 K, a small fraction of the α-particles recombine to produce nuclei in and slightly above the iron group: ^{56}Ni, ^{60}Zn, and ^{64}Ge. Flow beyond ^{64}Ge is inhibited, however, by strong reverse flows.

The second stage occurs as the temperature declines below $\sim 3 \times 10^9$ K. A combination of (n, p) and (p, γ) reactions carries the flow, still close to the $Z = N$ line, to heavier nuclei. For $A < 92$ the flow in the present calculations passes through the even-even $N = Z$ nuclei. After $N = Z = 44$ (^{88}Ru) the character of the flow changes. Effective synthesis of the next even-even nucleus (^{92}Pd) is prevented in part by the small proton separation energy of ^{91}Rh: the proton capture parent of ^{92}Pd. As in the analogous r-process, just how far the flow goes in a particular trajectory depends on the proton to seed ratio and especially on the number of neutrons per seed produced by $p(\bar{\nu}, e^+)n$. All interesting nuclei in this stage are made as proton-rich progenitors.

The third stage occurs as the temperature drops below 1.5×10^9 K and charged-particle reactions freeze out. Neutrons are still being produced by $p(\bar{\nu}, e^+)n$, however, albeit at a reduced rate (because both the neutrino luminosity declines and the distance to the neutron star is increasing). Now (n, p) reactions drive material toward the valley of beta stability. Because the nuclei involved are unstable to positron decay anyway, this only accelerates the inevitable. The atomic mass, A, does not change. It should be noted, however, that just as the r-process can contribute to nuclei made by the s-process that are unshielded against β^- decay of more neutron-rich isobars, so too can the $\nu - rp$ process considered here contribute to s-nuclei that are unshielded on the proton-rich side. That is, in addition to nuclei that are designated as "r, s," there may also be nuclei one should consider as "p, s."

The fourth stage only occurs in the most extreme situation, in which the number of neutrons produced by neutrinos is quite large compared with the number of seed nuclei. Then (n, p) reactions not only carry the flow at low temperature back to the valley of beta stability, but (n, γ) reactions carry it beyond—*to the neutron-rich side of the periodic chart*—even in the presence

of a large abundance of free protons. This is a novel version of the *r*-process that actually works best when the *proton* abundance is large but the temperature is too low for proton addition. The protons are just a source of neutrons.

3.2. *A Basic Parameter of the Process:* Δ_n

The most interesting part of the nucleosynthesis occurs during the later stages of the outflow as the material cools. In the absence of an important neutrino flux the final isotopic yields are determined by an interplay between (p, γ), (γ, p), and β^+ processes, as well as details of how these reactions fall out of equilibrium. When neutrino capture on free protons is important, nuclei are pushed to higher isospin and mass via (n, p) and (n, γ) reactions.

As a first approximation, neutrinos will be important if they create an appreciable number of neutrons per heavy nucleus. The ratio of created free neutrons to heavy nuclei is

$$\Delta_n = \frac{X_p n_\nu}{X_{\rm heavy}/\bar{A}} \approx 60 \frac{(2Y_e - 1)n_\nu}{1 - X_\alpha - X_p}, \tag{2}$$

where $X_{\rm heavy}$ is the mass fraction of elements heavier than α-particles and $\bar{A}$ is an effective average atomic number. The abundance of heavy nuclei in the outflow depends principally on the electron fraction, the entropy per baryon, and the expansion timescale characterizing the wind around the time of efficient α-particle formation. Hoffman et al. (1997) presented a study of the flow from helium to carbon that governs $X_{\rm heavy}$. Those authors found that the abundance of seed nuclei is essentially set by the time the temperature drops to 4 billion degrees. The simulations of Janka et al. (2003) follow the trajectories to a temperature that is lower than this, so the formation of seed nuclei at the most critical temperature is not sensitive to the extrapolation procedure. In addition, those simulations include relativistic effects that have been shown to have an important influence on characteristics of the wind at high temperatures (Cardall & Fuller 1997; Otsuki et al. 2000; Thompson et al. 2001). To give an indication of the sensitivity of $X_{\rm heavy}$ to the wind characteristics, we note that for a given free neutron fraction the abundance of heavy nuclei depends on $s^3/\tau_{\rm dyn}$ (Hoffman et al. 1997). That is, increasing the entropy or decreasing the dynamic timescale results in smaller production of seed nuclei and hence a larger number of free neutron captures per heavy nucleus.

In equation (2),

$$n_\nu = \int \lambda_{\bar{\nu}}\, dt \tag{3}$$

is the net number of neutrinos captured per free proton at temperatures smaller than about 3×10^9 K. Here

$$\lambda_{\bar{\nu}} \approx 0.06 \frac{L_{\bar{\nu}_e}}{10^{52}\ {\rm ergs\ s^{-1}}} \frac{T_{\bar{\nu}_e}}{4\ {\rm MeV}} \left(\frac{10^8\ {\rm cm}}{r}\right)^2 \tag{4}$$

is the rate at which each free proton captures $\bar{\nu}_e$ (Qian & Woosley 1996). In equation (4) $L_{\bar{\nu}_e}$ is the luminosity of electron antineutrinos, $T_{\bar{\nu}_e}$ is an effective temperature for these neutrinos, and r is the radius of the material from the $\bar{\nu}_e$ neutrino sphere.

To estimate the relation between Δ_n and nucleosynthesis, consider a mass element of unit volume comoving with the wind. The number of free protons in this mass element is

$$n_p = X_p \rho N_A. \tag{5}$$

TABLE 3

Neutron Absorption and Weak Decay Rates for Some Important Proton-rich Nuclei

Parent Nucleus	$\lambda(n, p)$[a]	$\lambda(n, \gamma)$[a]	$\lambda(\beta^+ + \text{electron capture})$[b]
^{64}Ge	6.4×10^8	4.5×10^5	0.01
^{66}As	7.7×10^8	9.6×10^5	7.24
^{68}Se	7.6×10^8	1.1×10^6	0.02
^{70}Br	1.0×10^9	2.0×10^6	8.67
^{80}Zr	1.6×10^9	4.5×10^6	0.18
^{116}Cd	3.3×10^{-13}	1.7×10^7	0.0

Note.—Taken from the statistical model calculations of Rauscher & Thielemann (2000).

[a] Stellar rate ($\rm cm^3\ mol^{-1}\ s$) at $T_9 = 2,\ \rho = 1\ \rm g\ cm^{-3}$.

[b] Weak rate in units of $\rm s^{-1}$.

These free protons are destroyed by antineutrino capture at a rate

$$\dot{n}_p = -n_p \lambda_{\bar{\nu}}. \tag{6}$$

Neutrons created when antineutrinos capture onto protons are subsequently absorbed by nuclei. The evolution of the free neutron abundance is then set by a competition between neutrino and nuclear processes,

$$\dot{X}_n = X_p \lambda_{\bar{\nu}} - \rho X_n \sum_i \frac{\lambda_i X_i}{A_i}. \tag{7}$$

Here the sum is over all isotopes i, and A_i and λ_i represent the atomic number and rate at which species i absorbs free neutrons. As a matter of convention λ_i here represents the rate at which a single atom of species i absorbs neutrons when the free neutron density is 1 mole per unit volume. If we introduce an average neutron absorption rate $\bar{\lambda}$, the destruction rate appearing on the right-hand side of equation (7) can be written

$$\sum \frac{\lambda_i X_i}{A_i} = X_{\rm heavy} \frac{\bar{\lambda}}{\bar{A}}. \tag{8}$$

Neutrons are principally absorbed in (n, p) and (n, γ) reactions, with (n, α) reactions playing a smaller role (due to the larger coulomb barrier in the exit channel). Table 3 shows rates for a sample of nuclei found in proton-rich outflows. At 2 billion degrees, typical values of λ_i for even-even proton-drip-line nuclei (those bordering the line separating the proton-bound nuclei from the proton-unbound nuclei) with mass near $A = 72$ are around 10^8–$10^9\ \rm cm^3\ mol^{-1}\ s$. This implies a very rapid neutron destruction rate. For example, at a typical density of $10^4\ \rm g\ cm^{-3}$ and a mass fraction of heavy nuclei equal to 10^{-3}, a neutron is absorbed in less than a microsecond. Since this is much shorter than the material expansion rate, it is fair to treat the neutron abundance as being in equilibrium,

$$X_n \approx \frac{X_p \lambda_{\bar{\nu}} \bar{A}}{\rho X_{\rm heavy} \bar{\lambda}}. \tag{9}$$

An estimate for the abundance of free neutrons also gives an estimate for the destruction rate of an atom of species i:

$$\dot{X}_i = -X_i X_n \lambda_i \rho \equiv -\tilde{\lambda}_i X_i. \tag{10}$$

Here we have defined an effective destruction rate that reflects the competition between different nuclear species for scarce neutrons,

$$\tilde{\lambda}_i = \left(\frac{100}{\text{s}}\right)\left(\frac{X_p \bar{A}}{10}\right)\left(\frac{10^{-2}}{X_{\text{heavy}}}\right)\left(\frac{\lambda_{\bar{\nu}}}{0.1\ \text{s}^{-1}}\right)\left(\frac{\lambda_i}{\bar{\lambda}}\right), \quad (11)$$

which is enormous. This equation says that for plausible outflow conditions, a given species can be entirely destroyed by neutrino-produced neutrons in times as short as $\sim$10 ms. It also implies a very small equilibrium neutron abundance: $X_N \lesssim 10^{-12}$ for $\rho \approx 10^4$ g cm^{-3}.

One of the most interesting questions relates to how high in mass the nucleosynthesis will proceed. For the purpose of making first estimates we can suppose the starting inventory of nuclei to be concentrated near mass 60. We also suppose that λ_i is independent of species for nuclei with $A \geq 60$. In this case the number of neutrons captured by a heavy nucleus is just Δ_n. A more careful treatment of λ_i is not presented, since results from detailed network-based calculations are given in § 3.3. With the above assumptions the mass fraction of species j to that of heavy nuclei is

$$\frac{X_j}{X_{\text{heavy}}} \approx \frac{\Delta_n^j}{j!} e^{-\Delta_n};\ j = N - 30. \quad (12)$$

Here we have defined a species to include all nuclei of a given isotone. Depending on just how fast the effective absorption rates $\tilde{\lambda}_i$ are, one might or might not suppose that decay of nuclei with odd-N is dominated by weak processes. This is because odd-N drip-line nuclei can have rather fast β^+ rates (see Table 3). When the neutron absorption rates are slower than these weak rates, one would take $j \approx (N - 30)/2$ in the above equation.

Although equation (12) is crude, it can be used as a rough guide to gauge the influence of free neutrons created from neutrino captures. As an example, suppose one neutron is created per heavy nucleus ($\Delta_n = 1$). In this case, equation (12) suggests that the relative mass fraction of nuclei that have captured a single neutron is about $1/e$, while the relative mass fraction of nuclei that have captured four neutrons is about 20 times smaller. If we use a factor of 10 decrease in mass fraction as a rough cutoff, this implies that an appreciable abundance of nuclei with mass up to $A \approx 60 + 4 \times 4 \approx 76$ will be synthesized. Here we have supposed that a unit increase in neutron number is accompanied by a unit increase in proton number. Neutron capture on odd-N proton-drip-line nuclei has been neglected, since the β^+ rates of these nuclei are much faster than the assumed neutron capture rate of $\sim$1 s^{-1}. As another example, suppose that $\Delta_n = 5$. In this case the relative mass fraction of nuclei that have captured five neutrons is about $20/e^5$, while the relative mass fraction of nuclei that have captured 11 neutrons is about 20 times smaller. This suggests appreciable synthesis of nuclei up to mass $A \approx 60 + 4 \times 11 \approx 100$. Here we have again assumed that the change in atomic number is twice the change in neutron number and that weak processes alone destroy odd-N nuclei. These assumptions probably lead to an overestimate for the increase in A in this case, because a neutron capture rate of $\sim$5 s^{-1} is comparable to the weak rates of many proton-drip-line nuclei.

The above considerations suggest a first constraint on conditions synthesizing p-nuclei with mass near 130,

$$\Delta_n \gtrsim 10. \quad (13)$$

A second constraint comes from considering the evolution of the outflow at low temperatures. As T falls below about 1.5×10^9 K, charged-particle capture rates begin to freeze out. Neutrons, on the other hand, are still rapidly absorbed. These neutron captures push the flow toward stability and away from progenitors of p-nuclei. If low-temperature neutrino-induced neutron production is significant, even the very neutron-rich r-process nuclei are synthesized. Minimal destruction of p-nuclei implies a second constraint,

$$\Delta_n(T \lesssim 1.5 \times 10^9) < \text{a few}. \quad (14)$$

Conversely, efficient synthesis of r-process isotopes in these proton-rich outflows requires the production of several neutrons per heavy nucleus at low temperatures.

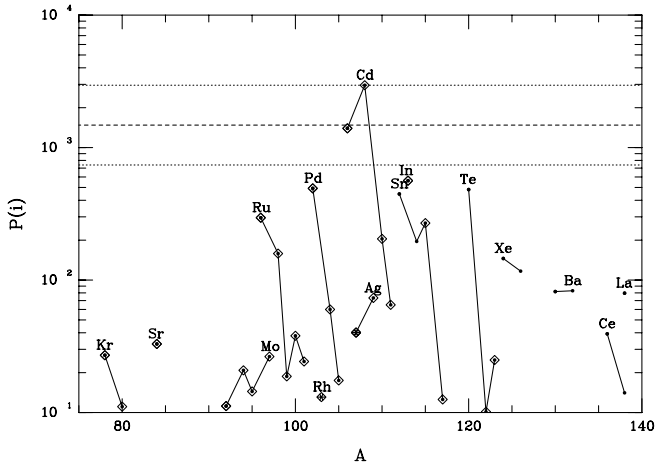

FIG. 4.—Integrated production factors calculated under the assumption that all six outflows comprising the early wind have twice the entropy found by Janka et al. (2003). Apart from the change in entropy, these outflows are assumed to have the same mass, electron fraction, and evolution of radius and temperature with time as the outflows represented in the middle panel of Fig. 1. The increase in entropy results in fewer seed nuclei, and values of Δ_n ranging from about 0.6 to 10.

3.3. *Results of Network Calculations*

Outflows characterized by the production of many free neutrons per heavy nucleus (large Δ_n) can be realized in different ways. For example, the timescale characterizing the expansion of the outflow around the time that α-particles are synthesized might be small, the flow might be held close to the neutron star for an extended period, or Y_e might be very large. For simplicity we consider implications of changing the entropy of the outflow (sensitivity to the outflow velocity, neutrino luminosities, and Y_e were treated earlier). Apart from the influence of neutrino captures occurring at low temperature, the precise mechanism by which Δ_n is increased is not so important for nucleosynthesis. Changes to the entropy of the hot bubble are not considered. Neutrino capture is not very pronounced in this portion of the outflow. Also, the hot bubble material does not begin close to the neutron star, so it is hard to see how an appreciable increase in the entropy of this material could be achieved.

Figure 4 shows the influence of doubling the entropy in the early wind. Like the middle panel of Figure 1, this figure gives integrated production factors for a wind comprised of six trajectories. Each of these trajectories has twice the entropy as, but is otherwise identical to, a counterpart trajectory from the simulation. For definiteness the increase in entropy was assumed to influence only the density evolution. The evolution of temperature with time was assumed to be the same as that found from simulation. To a fair approximation, doubling or tripling of the entropy corresponds to dividing the density by a factor of 2 or 3.

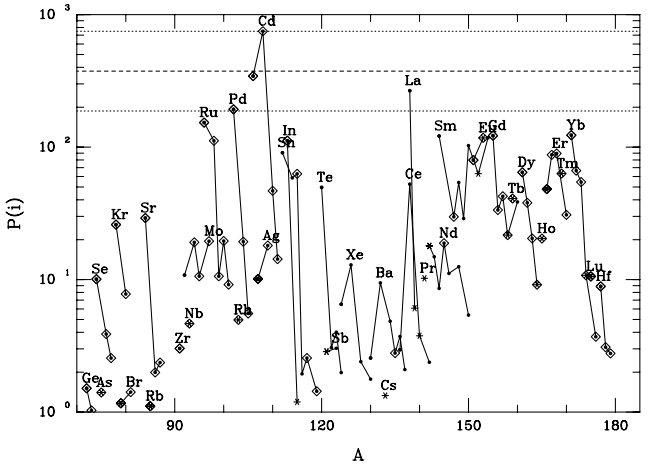

FIG. 5.— Integrated production factors calculated under the assumption that all six outflows comprising the early wind have 3 times the entropy found by Janka et al. (2003). Apart from the change in entropy, these outflows are assumed to have the same mass, electron fraction, and evolution of radius and temperature with time as the outflows represented in the middle panel of Fig. 1. For these very high entropy outflows Δ_n spans the range from 1 to 22.

Doubling the entropy in the early wind results in values of Δ_n ranging from about 0.6 to 10. The increased number of neutron captures results in efficient synthesis of nuclei as heavy as mass 125. By contrast, for all of the unmodified wind trajectories, Δ_n is less than about 3, and efficient synthesis stops around Ru and Pd.

Figure 5 shows the influence of tripling the entropy in the early wind. Again, this shows integrated production factors for six trajectories that each have larger entropy than, but are otherwise identical to, the unaltered trajectories described by the middle panel of Figure 1. These modified high-entropy wind trajectories have values of Δ_n ranging from about 1 to 22. This results in efficient synthesis of nuclei as heavy as mass 170. In other words, increasing the number of neutrons captured per heavy nucleus by 10 pushes the flow some 40 units higher in mass.

3.4. *Influence of Neutrino Capture at Low Temperatures*

Although outflows predicted by simulations have values of Δ_n that are too small to allow synthesis of $A \sim 130$ p-nuclei, they naturally satisfy the constraint (eq. [14]) on the relative number of neutrino captures occurring while the wind material is so cold that charged-particle captures have frozen out. Figure 6 shows the evolution of $\int dt/r^2$ as a function of temperature for the wind outflow of trajectory 6, characterized by $s/k_b \approx 77$ and $Y_e = 0.57$. It can be seen that the fraction of neutrino captures occurring at low temperatures (less than 1.5 billion degrees) is quite small, less than about 5%.

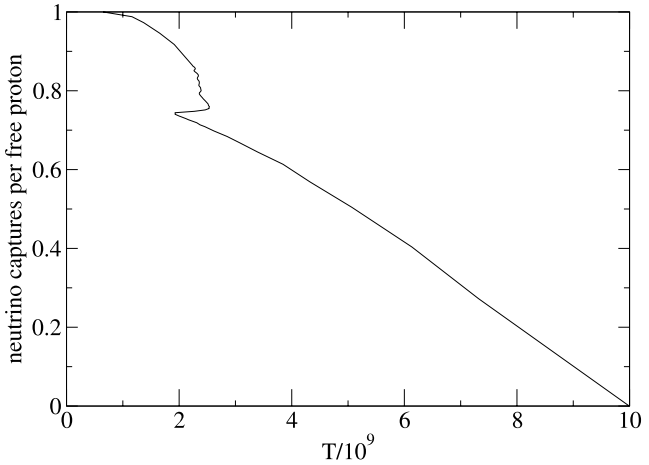

FIG. 6.— Evolution of the number of neutrino captures per free proton as a function of temperature in a wind trajectory calculated by Janka et al. (2003). This trajectory is characterized by $s/k_b \approx 77$ and $Y_e = 0.57$. The y-axis has been normalized to unity. Note that only a small fraction of the neutrino captures occur at low temperature.

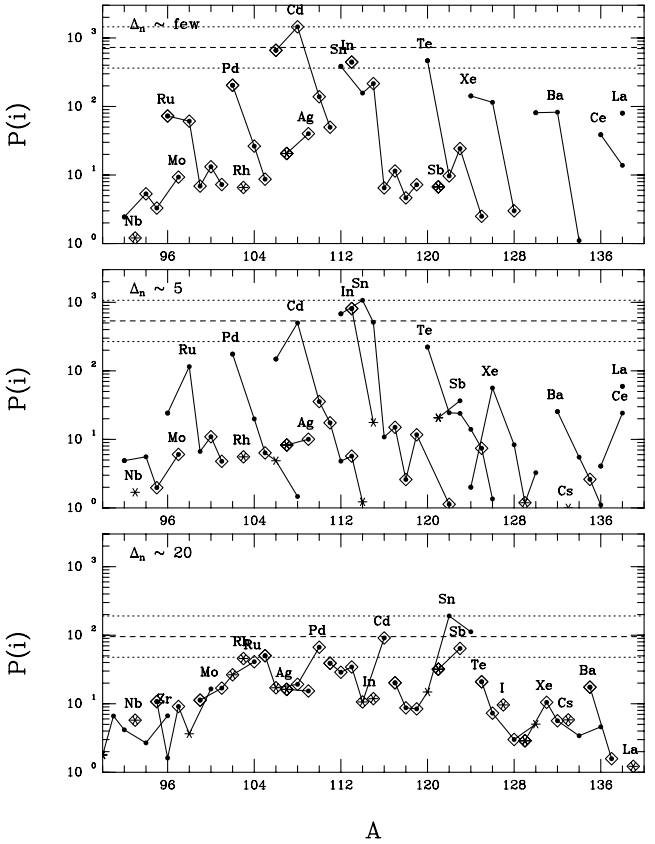

FIG. 7.— Influence of the weak production of neutrons at low temperatures on nucleosynthesis. *Top:* Nucleosynthesis in a trajectory with the nominal asymptotic radial velocity of 4×10^8 cm s^{-1}. This trajectory is characterized by the weak production of few neutrons per heavy nucleus at temperatures lower than 2×10^9 K. All dominant species are made as proton-rich radioactive progenitors. *Middle:* Nucleosynthesis in a trajectory characterized by the production of about 5 neutrons per heavy nucleus at temperatures lower than 1.5×10^9 K. Apart from having a smaller radius at low temperatures, this trajectory is identical to that represented by the top panel. It can be seen that the production of some p-nuclei (^{96}Ru and ^{114}Xe) has been greatly reduced. Nearly all species are made as themselves. *Bottom:* Nucleosynthesis in a trajectory characterized by the production of about 20 neutrons per heavy nucleus at temperatures lower than 1.5×10^9 K. Apart from the radius/time history, this trajectory is identical to that represented by the other two panels. For this case, where many neutrons are captured at low temperatures, all major species have neutron-rich progenitors, allowing for the production of the r-only species ^{110}Pd, ^{116}Cd, and ^{122,124}Sn.

To illustrate the influence of neutrino captures occurring while the outflow is cold enough that charged-particle reactions have frozen out, we modified the entropy-doubled version of trajectory 6 (see Table 2) to be held close to the neutron star at temperatures less than 1.5 billion degrees. Results are shown in Figure 7. The top panel here shows nucleosynthesis in an outflow with the nominal value for the asymptotic radial velocity (4×10^8 cm s^{-1}). The dominant production factors are for the p-isotopes of Ru, Pd, and Cd. In this trajectory these nuclei are not synthesized as themselves, but as more proton-rich unstable isotopes.

A relatively modest modification to the outflow results in the capture of about five neutrons per heavy nucleus at temperatures

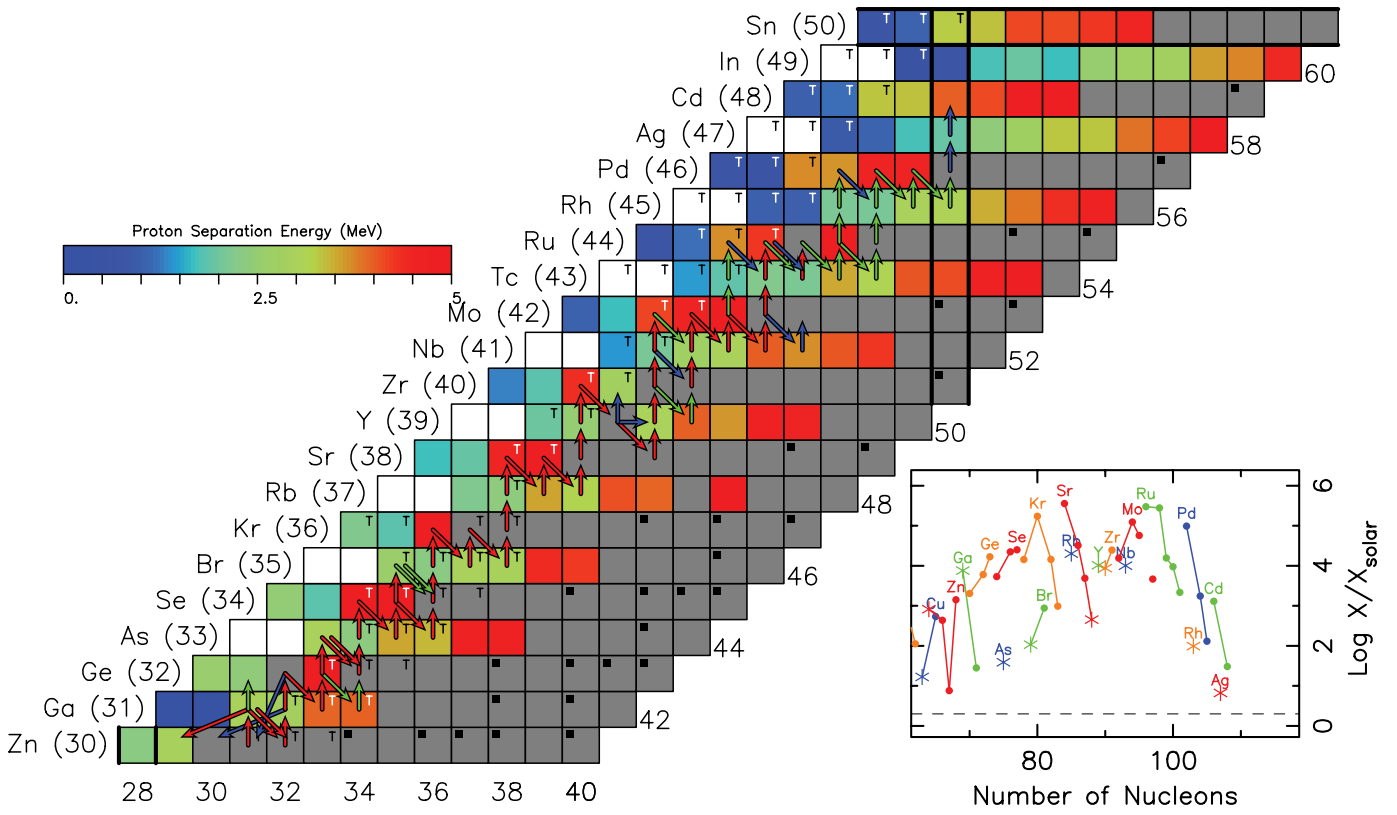

FIG. 8.—Net nuclear flows in the (Z, N) plane from zinc to tin when material in the unmodified wind outflow of trajectory 6 has a temperature $T_9 = 2.05$ and density $\rho = 2.7 \times 10^4$ g cm^{-3}. The net nuclear flow (in units of s^{-1}) is defined as the product of abundance, density, and reaction rate in the forward (charge or mass increasing) direction minus a similar quantity for the inverse reaction. Strong and electromagnetic flows begin at the center of a target nucleus and end as an arrow in the product nucleus. Any flow that starts off center represents weak decay. Net nuclear flows are plotted in three strengths: red (strong), green (intermediate), and blue (weak), with values that are between a factor of 1.0 to 0.1, 0.1 to 0.02, and 0.02 to 0.01 of the value of the largest flow in the figure, respectively. The largest flow here is ^{61}Zn(p, γ) ^{62}Ga$(1.75 \times 10^{-4}$ s$^{-1})$. Stable species are represented by a filled black square in the upper left corner. Each nucleus is color coded according to the legend by the value of its proton separation energy. Proton unbound nuclei are colored white. Nuclei with $S_p > 5$ MeV are colored gray. A "T" is plotted in the upper right-hand corner for nuclei whose binding energy was extrapolated from measured masses (Audi & Wapstra 1995). Production factors at the time shown are given in the inset (the stable isotopes depicted include the abundances of all radioactive progenitors that will eventually decay to them). As discussed in the text, the classical *rp*-process waiting points (^{64}Ge, ^{68}Se, ^{72}Kr, and ^{76}Sr) are bypassed by (n, p) reactions.

lower than 1.5×10^9 K. The middle panel of Figure 7 shows nucleosynthesis in such a trajectory. The largest overproductions have shifted to the heavier *p*-nuclei of Sn, but the *p*-nuclei of Ru and Xe have been reduced, and all species are now being made as themselves. Since the only difference between the trajectories represented by the middle and top panels of Figure 7 is the evolution of radius with time at low temperatures, all differences in nucleosynthesis arise from late-time neutron production. It is seen that a couple of neutrons produced at the wrong time can be detrimental to the synthesis of some *p*-process isotopes.

The bottom panel of Figure 7 shows the influence of a great number of neutrons produced at low temperatures. Again, this was studied by modifying just the radial profile at temperatures less than 1.5 billion degrees of the entropy-doubled version of trajectory 6. In this trajectory about 20 free neutrons are created per heavy nucleus at low temperatures. The radioactive progenitors of Ru, Pd, and Cd are now all neutron-rich, providing for the production of the *r*-only nuclei ^{110}Pd, ^{116}Cd, and $^{122, 124}$Sn. It is perhaps remarkable that some second-peak *r*-isotopes can be synthesized in these proton-rich environments. It may be difficult, however, to have ejecta that are both cold enough and close enough to the neutron star to experience the necessary neutrino irradiation.

3.5. *Details of the Nuclear Flows*

In all trajectory studies, regardless of initial electron fraction or entropy, nucleosynthesis begins with ^{12}C produced early-on by the reaction sequence $\alpha(\alpha n, \gamma)$ ^{9}Be(α, n) ^{12}C. By the time $T_9 \sim 3$ the iron group has already been assembled. Strong (α, γ) and pairs of (p, γ) and (α, p) reactions continue to populate the even-*Z* even-*N* α-nuclei up to ^{56}Ni and ^{60}Zn. The flow mostly travels along the $Z = N$ line and does not stray more than two neutrons from it for any element up to zinc. This continues until the charged-particle reactions freeze out ($T_9 \sim 1.5$).

Characteristics of the nucleosynthesis at lower temperatures depend sensitively on the influence of neutrino captures. To illustrate the influence of $p(\bar{\nu}_e, e^+)n$ reactions, we begin with a discussion of nucleosynthesis in trajectory 6, which is characterized by the weak production of a few neutrons per heavy nucleus. Important nuclear flows occurring when material in this trajectory has a temperature $T = 2.05 \times 10^9$ K are shown in Figure 8. It can be seen that the dominant flows (*red arrows*) are due to proton-capture (p, γ) reactions. These can proceed until a proton unbound (*denoted by a white square*) or small (*blue*) proton separation energy (S_p) is encountered. Unlike the *rp*-process, here we have a neutron abundance and, although small, it allows (n, p) reactions to populate the next lowest isobar. The (p, γ) flow is governed by the separation energies.

The end result for this trajectory is the production of the light *p*-process nuclei from Kr to Pd. The (n, p) reactions can continue to carry the flow even at low temperatures, because such reactions on targets a few neutrons to the proton side of stability typically have positive *Q* values (i.e., no thresholds). The flow to

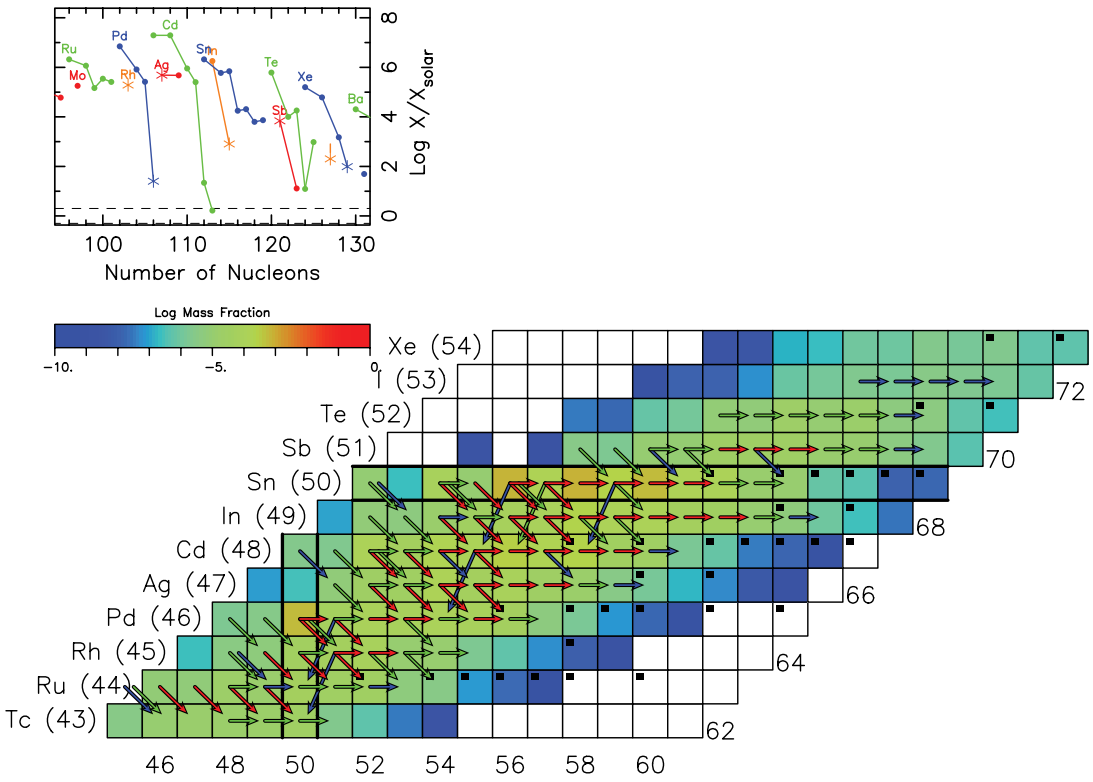

FIG. 9.—Net nuclear flows from technetium to xenon in the modified (entropy-doubled) wind trajectory with $Y_e = 0.570$. At the time shown here $T_9 = 1.01$, $\rho = 1.2 \times 10^3$, and $Y_e = 0.561$. The reactant mass fractions are $X(p) = 0.122$, $X(n) = 10^{-12}$, and $X(\alpha) = 0.865$. The flows are depicted exactly as in Fig. 8; at this time, the largest flow is ^{109}Sn(n, γ) ^{110}Sn$(7.91 \times 10^{-7}$ s$^{-1})$. Each isotope is color coded according to the legend by the logarithm of its mass fraction; the largest at this time is $X(^{108}\mathrm{Sn}) = 7.1 \times 10^{-4}$. The charged-particle reactions have frozen out, leaving (n, p) and (n, γ) reactions to carry the flow rapidly toward stability (before the onset of weak decay). This allows p-nuclei such as ^{112}Sn and ^{120}Te to be made as themselves via neutron capture reactions.

heavier nuclei eventually stops when the charged-particle reactions freeze out ($T_9 \leq 1.5$) and at late times (once the waiting points are passed) when (n, p) and (n, γ) reactions (or weak decay) direct the flows toward stability.

An interesting although unfortunate occurrence is the low (relative to Ru and Pd) production of the most abundant p-nucleus in nature, ^{92}Mo. As the proton capture flow moves up the $N = 46$ isotones (see Fig. 8) it is stopped in part because ^{91}Rh has a small proton separation energy. This prevents efficient population of ^{92}Pd ($Z = N = 46$) and so breaks the pattern of synthesizing the even-even $N = Z$ nuclei. As a consequence, the flow detours toward stability until reaching $N = 47$ and 48. The result is that the radioactive progenitor for ^{92}Mo is now the odd-odd nucleus ^{92}Rh. The flow moves very quickly through this nucleus (as well as through ^{92}Ru), and little is left for decay at the end of this trajectory.

It is notable that the heavier p-nuclei, ^{96,98}Ru and ^{102}Pd, are coproduced in amounts that might explain their solar abundances. Their radioactive progenitors are associated with nuclei in the two nearby closed shells. Heavier p-nuclei (^{102}Cd, etc.) are not made here because the flow failed to populate isotopes in the $Z = 50$ proton shell. ^{92}Mo is the only one of these intermediate p-nuclei that (for now) appears to have an odd-Z progenitor. We note, however, that the flow goes through regions where the possible error on S_p is potentially large (indicated by the T, meaning the value of S_p was from an extrapolation from measured values). More accurate measurements here would be most welcome and could have significant impact on our understanding of p-process nuclei and their solar abundances, since this material is ejected (unlike the case in X-ray bursts). As an example, the uncertainty in the proton separation energy of ^{91}Ru is about 600 keV. A plausible 1 MeV increase in this separation energy results in a 50% increase in the yield of ^{92}Mo in trajectory 6.

Figure 9 shows nucleosynthesis in a trajectory characterized by the production of many free neutrons per heavy nucleus. This trajectory has an initial electron fraction $Y_e = 0.570$ and entropy $s/k_b \approx 148$. It was constructed by doubling the entropy in the two-dimensional simulation of trajectory 6 (Table 2). For this modified outflow $\Delta_n \approx 22$.

When material in this modified trajectory reaches a temperature of about $T_9 \sim 2$, (p, γ) reactions on ^{110}Sn (with $S_p \geq 5$ MeV) pierce the $Z = 50$ closed proton shell. At the time shown in Figure 9 (2.21 s, $T_9 = 1.01$), the charged-particle reactions have frozen out, but the flow has entered an area where weak decay has yet to dominate. Instead, (n, p) and (n, γ) reactions carry the flow rapidly toward stability. The p-nuclei of Ru, Pd, and Cd are all made as radioactive progenitors in the closed neutron (Ru) and proton (Pd and Cd) shells. We are in a very novel regime, where one can synthesize p-nuclei (such as ^{112}Sn and ^{120}Te) via neutron capture reactions.

4. CONCLUSIONS

Current supernova simulations, without modification, provide the necessary conditions required to produce a number of p-process isotopes whose origin in nature has always been unclear. The site is the proton-rich bubble that powers the explosion and the early neutrino-powered wind that develops right behind it. The synthesis is primary, so a neutron star derived from a metal-poor progenitor star would produce the same yields (as long as the neutron star itself had the same properties). Very

metal-deficient stars formed from these ejecta would be characterized by an excess of both *p*-process nuclei and *r*-process nuclei compared to the *s*-process, but since there is no element that is dominantly *p*-process, observational diagnostics may be difficult.

In particular, large quantities of ^{96,98}Ru and ^{102}Pd are produced in our calculations (Fig. 1). This may be interesting because some tentative lines of evidence indicate that these isotopes do not follow the same trends as other *p*-process nuclei. Hayakawa et al. (2004) studied the ratios of the solar abundances of *p*-nuclei relative to the solar abundances of their more neutron-rich progenitors [represented in their paper by $N(s)/N(p)$] in the γ-process. Those authors point out that if *p*-nuclei really are produced in the γ-process, then there ought to be some correlation between the *p*-nuclei and their progenitors. And indeed a nearly constant value for $N(s)/N(p)$ is found for most of the *p*-nuclei whose parents were completely or nearly completely synthesized in the *s*-process. However, for ^{96,98}Ru they found that $N(s)/N(p)$ is lower than the average by about a factor of 4, while for ^{102}Pd this ratio is lower than the average by about a factor of 2. The proton-rich Ru isotopes have been historically underproduced in many calculations, while ^{102}Pd tends to be underproduced by about a factor of 3, although its yield is quite sensitive to seed abundances (Woosley & Howard 1978; Prantzos et al. 1990; Rayet et al. 1995). From a microphysics perspective, the relative abundances of *p*-nuclei produced in the γ-process are largely a consequence of the photodissociation trends for these nuclei and their progenitors (Woosley & Howard 1978). The anticorrelation between photodissociation rates and abundances of *p*-nuclei was used as an argument in favor of secondary production. Although this is not observational evidence that a particular nuclide was synthesized in the γ-process, it strongly suggests that a great swath of them were. That detailed simulations of the γ-process show a relative underproduction of the *p*-isotopes of Mo, Ru, and Pd suggests that the microphysics governing photodissociation rates is not enough to explain the abundances of these nuclei.

Synthesis of *p*-process isotopes as heavy as ^{120}Te can also be achieved by only factor-of-2 modifications to the entropy of our baseline simulation. It is interesting to note in this regard that an even larger increase in entropy is needed later in the *neutron*-rich wind for the efficient synthesis of the *r*-process isotopes (e.g., Qian & Woosley 1996). This is quite possibly informing us of some additional heating mechanism that operates in the mass outflow during the first few seconds of a neutron star's life. Possible mechanisms are magnetic field entrainment of the outflowing matter (Thompson 2003), magnetic energy dissipation (Qian & Woosley 1996), acoustic energy input (Qian & Woosley 1996; Burrows et al. 2006), or Alfvén wave dampening (Suzuki & Nagataki 2005). None of these were included in the present supernova model, but we varied the entropy to determine qualitatively their effect.

In the more extreme but still physically reasonable case that the entropy is multiplied by 3, the synthesis extends all the way to ^{168}Yb, with the accompanying production of many isotopes normally attributed to the *s*-process and even the *r*-process.

It is somewhat disappointing that none of our calculations produce a large overabundance of ^{92}Mo compared to surrounding isotopes (although some do make 10% of the necessary value). This may reflect the fact that ^{92}Mo has another origin, e.g., the same neutrino-powered wind a few seconds later, when $Y_e = 0.485$. As Hoffman et al. (1996; see their Fig. 3) found that winds that efficiently synthesize ^{92}Mo cannot also synthesize ^{96,98}Ru, ^{102}Pd, or even ^{94}Mo, production of ^{92}Mo in a neutron-rich outflow would not conflict with production of the *p*-isotopes efficiently synthesized in our calculations of proton-rich winds. Underproduction of ^{92}Mo in the current simulations may also reflect uncertainties in the nuclear physics. In the current study, the ^{92}Mo that is made is produced as the odd-odd progenitor ^{92}Rh. This does not take advantage of the extra stability that would be afforded by an even-even nucleus such as ^{92}Pd, let alone the magic neutron shell of ^{92}Mo itself. Indeed, the binding energies and lifetimes of nuclei in the vicinity of ^{92}Pd are quite uncertain.

An important aspect of the synthesis calculated here is that none of the *p*-nuclei are made as themselves; all have proton-rich progenitors. Many of these progenitors are so unstable that even their masses and lifetimes are not measured, let alone their cross sections for interacting with neutrons and protons. A similar situation is encountered in the *rp*-process in type I X-ray bursts (e.g., Schatz et al. 2001), a critical difference being that the isotopes made here are actually ejected and contribute to the solar inventory of heavy elements. The study of these is a major goal for nuclear astrophysics experiments of the future, such as the Rare Isotope Accelerator.[1] For now, we can only note that these nuclear uncertainties are almost certainly responsible for a large fraction of the spread in production factors in, e.g., Figures 1 and 4.

This study has explored only a relatively limited set of outflow parameter space based on simple modifications to trajectories found in one particular supernova simulation. Further studies will surely be carried out by us and others, but we have identified a key physical parameter, Δ_n (eq. [2]), which characterizes the solution for various combinations of timescale, Y_e, and entropy; Δ_n is essentially a dimensionless measure of the number of neutrons produced by neutrino capture on protons compared to the number of heavy seed nuclei. Surveys on a finer grid of Δ_n than were used here will be interesting.

This work was performed under the auspices of the US Department of Energy by the University of California Lawrence Livermore National Laboratory, under contract W-7405-ENG-48. It was also supported in part by the SciDAC Program of the US Department of Energy (DC-FC02-01ER41176), the National Science Foundation (AST 02-06111), and NASA (NNG 05-GG08G), and, in Germany, by the Research Center for Astroparticle Physics (SFB 375) and the Transregional Collaborative Research Center for Gravitational Wave Astronomy (SFB-Transregio 7). We would like to thank K. Kelley for insightful discussions.

[1] See http://www.anl.gov/ria/index.html.

REFERENCES

Arnould, M. 1976, A&A, 46, 117
Audi, G., & Wapstra, A. H. 1995, Nucl. Phys. A, 595, 409
Buras, R., Rampp, M., Janka, H.-T., & Kifonidis, K. 2006, A&A, 447, 1049
Burbidge, E. M., Burbidge, G. R., Fowler, W. A., & Hoyle, F. 1957, Rev. Mod. Phys., 29, 547
Burrows, A., Livne, E., Dessart, L., Ott, C., & Murphy, J. 2006, ApJ, 640, 878
Cardall, C. Y., & Fuller, G. M. 1997, ApJ, 486, L111
Duncan, R. C., Shapiro, S. L., & Wasserman, I. 1986, ApJ, 309, 141
Fröhlich, C., et al. 2004, Nucl. Phys. A, 758, 28c
———. 2006, ApJ, 637, 415
Fuller, G. M., & Meyer, B. S. 1995, ApJ, 453, 792
Hayakawa, T., Iwamoto, N., Shizuma, T., Kajino, T., Umeda, H., & Nomoto, K. 2004, Phys. Rev. Lett., 93, 161102

Hoffman, R. D., Woosley, S. E., Fuller, G. M., & Meyer, B. S. 1996, ApJ, 460, 478
Hoffman, R. D., Woosley, S. E., & Qian, Y.-Z. 1997, ApJ, 482, 951
Janka, H.-T., Buras, R., & Rampp, M. 2003, Nucl. Phys. A, 718, 269
Jordan, G. C., & Meyer, B. S. 2004, ApJ, 617, L131
Lodders, K. 2003, ApJ, 591, 1220
Mathews, G. J., Bazan, G., & Cowan, J. J. 1992, ApJ, 391, 719
McLaughlin, G. C., & Fuller, G. M. 1995, ApJ, 455, 202 (erratum 466, 1100 [1996])
Meyer, B. S. 1995, ApJ, 449, L55
Otsuki, K., Tagoshi, H., Kajino, T., & Wanajo, S. 2000, ApJ, 533, 424
Prantzos, N., Hashimoto, M., Rayet, M., & Arnould, M. 1990, A&A, 238, 455
Pruet, J., Woosley, S. E., Janka, H.-T., Buras, R., & Hoffman, R. D. 2005, ApJ, 623, 325
Qian, Y.-Z., & Woosley, S. E. 1996, ApJ, 471, 331
Rauscher, T., Heger, A., Hoffman, R. D., & Woosley, S. E. 2002, ApJ, 576, 323
Rauscher, T., & Thielemann, F.-K. 2000, At. Data Nucl. Data Tables, 75, 1
Rayet, M., Arnould, M., Hashimoto, M., Prantzos, N., & Nomoto, K. 1995, A&A, 298, 517
Schatz, H., et al. 2001, Phys. Rev. Lett., 86, 3471
Suzuki, T. K., & Nagataki, S. 2005, ApJ, 628, 914
Thompson, T. A. 2003, ApJ, 585, L33
Thompson, T. A., Burrows, A., & Meyer, B. S. 2001, ApJ, 562, 887
Woosley, S. E., Hartmann, D. H., Hoffman, R. D., & Haxton, W. C. 1990, ApJ, 356, 272
Woosley, S. E., Heger, A., & Weaver, T. A. 2002, Rev. Mod. Phys., 74, 1015
Woosley, S. E., & Howard, W. M. 1978, ApJS, 36, 285
Woosley, S. E., & Weaver, T. A. 1995, ApJS, 101, 181
Woosley, S. E., Wilson, J. R., Mathews, G. J., Hoffman, R. D., & Meyer, B. S. 1994, ApJ, 433, 229